Aiming at understanding thermo-mechanical loads in the first wall of DEMO: Stress-strain evolution in a Eurofer-tungsten test component featuring a functionally graded interlayer

S. Heuer[a,*], Th. Weber[a], G. Pintsuk[a], J.W. Coenen[a], J. Matejicek[b], Ch. Linsmeier[a]

[a] *Forschungszentrum Jülich GmbH, Institut für Energie- und Klimaforschung - Plasmaphysik, Partner of the Trilateral Euregio Cluster (TEC), 52425 Jülich, Germany*

[b] *The Czech Academy of Sciences, Institute of Plasma Physics, 18200 Prague, Czech Republic*

Abstract

For the future fusion demonstration power plant, DEMO, several blanket designs are currently under consideration. Despite geometric and operational differences, all designs suggest a first wall (FW), in which tungsten (W) armour is joined to a structure made of Reduced Activation Ferritic Martensitic (RAFM) steel. In thermo-mechanical analyses of breeding blankets, this joint has received limited attention. In order to provide a basis for better understanding of thermally induced stresses and strains in the FW, the thermo-mechanical behaviour of a water-cooled test component is explored in the current contribution. The model aims at providing a simple geometry that allows straightforward comparison of numerical and experimental results, while trying to keep boundary conditions as realistic as possible. A test component with direct RAFM steel-W joint, and a test component with a stress-redistributing, functionally graded RAFM steel/W interlayer in the joint is considered in the current contribution. The analyses take production- and operation-related loads into account. Following a detailed analysis of the evolution of stress components and strain in the model, a parameter study with respect to geometric specifications and loads is presented.

The analyses show that, even in a small test component, a direct RAFM steel-W joint causes enormous plastic deformation. The implementation of a functionally graded interlayer reduces stresses and strains significantly, but vertical normal stresses at the joint's circumference remain considerable. With the component geometry considered here, the graded interlayer should be at least 1 mm thick and contain 4 sublayers to appropriately redistribute stresses. Beyond a component width of 14 mm, stresses increase strongly, which may pose a risk to the applicability of large-scale FW components, too.

Keywords:
nuclear fusion, DEMO, first wall, Finite Element Analysis, functionally graded materials (FGM), Fe/W

1. Introduction

The first wall (FW) of future fusion reactors like DEMO will likely be realized of mixed-material components. While tungsten (W) is a promising plasma facing material due to its thermal and physical properties [1], a high neutron capture cross section and long cooling down time, required before maintenance, limits its thickness to af few millimetres [2]. Suitable FW structural materials, that the W armour is attached to, are summarised as the group of Reduced Activation Ferritic Martensitic (RAFM) steels, among them Eurofer and F82H [3]. Due to the discrete transition of material properties accompanying a macroscopically direct RAFM steel-W joint, localised loads at the interface are generated in production and operation. In particular, these loads are thermally induced macroscopic stresses and strains arising from different coefficients of thermal expansion, α. Thermally induced stresses and strains may either spontaneously or in the long term yield pre-mature failure of the FW component requiring feasible ways to reduce the loads [4, 5]. For W and Eurofer (representing the class of RAFM steels here), α is given in tabs. 1 and 2 along with other temperature dependent materials properties used in this work.

Several approaches to create resilient RAFM steel-W joints are currently being investigated. Implementing a vanadium foil ($\alpha_V \approx 8,4 \cdot 10^{-6}$ K^{-1}) in the joint could reduce the mismatch of thermal expansion between RAFM steel and W, and make the production technique (uniaxial hot pressing) possible at fairly low temperatures (700°C) [6–10]. However, this results in formation of the brittle σ phase FeV during subsequent ageing [10]. An additional Ti foil ($\alpha_{Ti} \approx 8,6 \cdot 10^{-6}$ K^{-1}) in between the RAFM steel part and the V foil delivers favourable properties at the V side and is an effective diffusion barrier preventing the formation of FeV [10–12]. Yet, in this layered system, other brittle intermetallic precipitates like Fe_2Ti- and FeTi establish during uniaxial hot pressing [11, 12] and hot isostatic pressing [13–15]. Weakening intermetallic precipitates were also observed for other approaches, e.g. replacing the Ti foil by Ni [16] or using only a Ni interlayer [17]. Cu based interlayers ($\alpha_{Cu} \approx 16,5 \cdot 10^{-6}$ K^{-1}), e.g. realized by Cai et al. and Pintsuk et al. [18, 19], show good bonding to steel and W, but may be unsuitable for high FW heat loads due to low solidus temperatures and high plastic strains, causing failure upon cyclic loading. Brazing of fusion relevant components is generally

*Corresponding author
Email address: s.heuer@fz-juelich.de (S. Heuer)

problematic as most investigated brazes based on Cu, Ag, or Ni develop long-living radionuclides under fusion relevant neutron loads. Work done by Chehtov, Kalin and Ma [20–23] in addition reveals weak features like partial recrystallization of the steel, intermetallic precipitates or pores along the joints.

Summarising the aforementioned aspects, none of the named interlayer systems is technologically reliable yet to join RAFM steel and W, and effectively reduce stresses and strains within a FW component. Functionally graded RAFM steel/W materials (in the following: FGMs) are another promising interlayer option. The class of materials exhibits a compositional grading across the material's height. Given this, RAFM steel/W FGMs are able to gradually approximate homogenized materials properties, such as the coefficient of thermal expansion, across the FGM layer's height and, thus, smoothly re-distribute macroscopic stresses. The combination of W and Fe base materials may be accompanied by the formation of brittle intermetallic phases, Fe_7W_6 and Fe_2W [4, 24], similar as to the above named interlayer developments. Yet, to date these phases do not seem to harm the joint more than precipitates observed in the other interlayer developments while favourably simplifying the material mix within the FW component. The latter may in particular be interesting for recycling of activated and transmuted FW components. Moreover, FGMs may re-distribute and level macrostresses more smoothly compared to homogeneous interlayers. Localised microstress peaks may still be present, particularly in powder metallurgically produced FGMs, containing both pure RAFM steel and W volumes. However, microstresses abate within very short distances, e.g. the mentioned pure volumes, instead of superposing along the macroscopically flat interface of a direct RAFM steel-W joint like macrostresses do.

Several studies on the processing and the impact of FGMs for Cu-W and RAFM steel-W joints of different divertor designs, e.g. the thin-walled finger module design, were already carried out with experimental [7, 19, 25–32] and numerical [33–35] approaches. In contrast, FGMs particularly used for larger-area RAFM steel-W joints of the FW have received less consideration, only by Qu [36–38] and Emmerich [39]. Qu introduced a 2D model (plane strain) of a rectangular piece of the FW with variable FGM thickness. The model takes elasto-plastic and elasto-viscoplastic material properties into account, but neglects cooling and assumes a homogeneous temperature field [36]. Emmerich further developed the aforementioned model towards a more realistic geometry of the FW. While a greater plate with several cooling pipes allows the consideration of an inhomogeneous temperature field across the FW, the model does not include an FGM thickness variation [39]. Both models take fabrication-related loads into account, but they apply fixed temperatures as boundary conditions (decoupled from operational heat loads) and focus on von Mises stresses and plastic deformations of the W-FGM-Eurofer joint in a central region of the FW (away from edges) over the FW lifetime.

The present contribution tries to support the understanding of DEMO FW loads by filling a gap between the two described models. For that, a test component, similar to a divertor monoblock, which is in between the complexities of the named models, is considered. This design allows straightforward comparison of the numerical results to experimental data of a simple test component, meaningful variation of geometric boundary conditions (FGM thickness, number of FGM sublayers, component size) and dedicated consideration of the edge effect of the W-FGM-Eurofer joint. With respect to the latter, the selected geometry is analysed with and without FGM, and the discussion of the von Mises stress evolution over the lifetime is supported by normal and shear stresses. Temperatures are related to different heat fluxes and to water cooling capabilities.

Modelling in the present work is carried out in three steps. First, suitable FGM properties models are selected, secondly, relevant stress components and the equivalent plastic strain of the first load cycles within the test component are analysed in detail. Lastly, parameter studies are carried out that analyse the number of FGM sublayers, the FGM thickness, the selected component size and different heat loads.

2. FE model

In this section, first, the geometry of the modelled component and boundary conditions are described, followed by the selection of material property models for the FGM.

2.1. Geometry and boundary conditions

In the current work, the 2D geometry of a test component, depicted in fig. 1, was modelled, similar to the geometry used by Igitkhanov [40, 41]. Thermo-mechanical analysis of the geometry aims at understanding the stress-strain evolution in a Eurofer-W component with and without FGM with respect to FW heat loads of the second operational phase of DEMO. Since no blanket design for DEMO is selected yet, and a realistic (complex) representation of the FW complicates straightforward comparison of the numeric results to future experimental test results of a real component, the depicted simplified geometry was selected. For computational efficiency only half of the geometry was realized and a vertical symmetry axis was included.

The geometry consists of three components, each inseparably bonded to the adjacent. While the top and bottom pieces refer to standard tungsten and Eurofer parts made from bulk material with properties as given in tables 1 and 2, the centre piece describes a virtually ideal FGM. It is characterized by a quasi-linear volumetric grading of the pure constituents and, correspondingly, by a grading of their properties as described in subsection 2.2.

The W piece is set to 3 mm thickness in the present work. While the W armour thickness is limited to 2 mm in the reference component by Igitkhanov [41], recent studies on the erosion of DEMOs FW have shown that the W loss strongly depends on the scrape-off layer (SOL) clearance. Taking a low clearance like in ITER (Δ_{SOL} = 5 cm) into account, the W erosion equals 0.54 mm per full power year (fpy) [42]. Greater clearances cause lower, yet still significant erosion [43]. Considering an anticipated blanket lifetime of 5 fpy in DEMOs second operational phase (for which FGMs may be relevant),

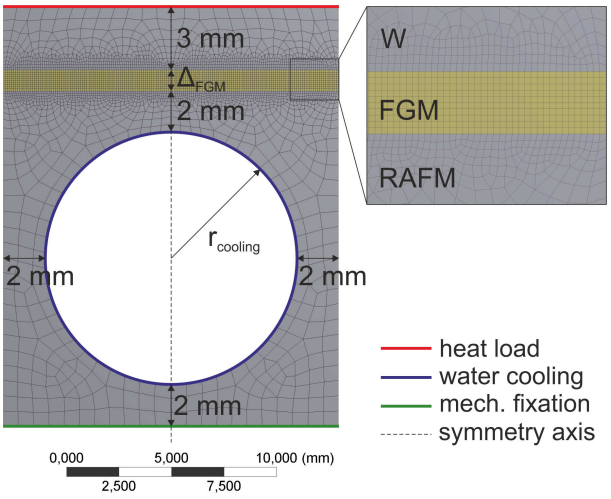

Figure 1: Geometry, boundary conditions and exemplary mesh of the modelled test component. For picturing reasons, in the FGM part only one percent of the generated elements are depicted.

uncertainties about the DEMO SOL and erosion safety factors that will probably have to be taken into account, the present study regards an increased, conservative W thickness of 3 mm. Generally, thicker W armour may be problematic due to strong neutron capture, which lowers the tritium breeding ratio.

The Eurofer part of the present study exhibits a quadratic cross section with a circular cooling structure. Usually, rectangular cooling structures are assumed for implementation in the FW and are modelled e.g. in [39, 41], but with respect to comparing numerical results to future experimental results, a circular cooling pipe is easier to machine and hence applied here. Width of the entire component and height of the Eurofer piece are commonly varied from 12 to 24 mm in the context of a parameter study to gain knowledge about a size effect. The cooling structure was adjusted correspondingly, giving a consequent minimum wall thickness of the Eurofer part of 2 mm.

The FGM layer is implemented as an additional part instead of replacing portions of the W and/or Eurofer parts. This increases the component thickness compared to Igitkhanov's geometry [40, 41]. Based on a conservative evaluation of the applicability of the FGM layer in the FW, load bearing duties of the steel structure were decided not to be transferred to the functional interlayer. This requires the thickness increase of the FGM-featured model, which is also most conservative with respect to heat removal capabilities. The FGM thickness is varied within another parameter study between 0.3 and 3 mm.

Thermo-mechanical modelling was carried out using the software Ansys. Elements of type PLANE223 were selected within a plane-stress, transient structural analysis environment. It should be noted here, that the plane-stress approach is rather optimistic compared to reality, whereas the plane-strain approach overestimates stresses in components of limited dimensions. Mechanical boundary conditions were applied to the bottom edge of the geometry in the term of suppression of vertical movement of nodes, and by adding the symmetry axis. This behaviour allows horizontal expansion of the geometry and prohibits bending. It is assumed to occur in an experimentally tested component, bonded to a base plate, as well as in the FW, which is bonded (mechanically coupled) to the blanket.

Thermal boundary conditions were applied to the surface of the cooling pipe and to the surface of the W tile. For the cooling pipe an adjusted heat transfer coefficient between the RAFM steel and the coolant was set. Coolant conditions were approximated simplifying Di Maio's and You's suggestions for a water cooled divertor cassette [46, 47]. In the present work, the water temperature is assumed to be 200°C, the pressure 3.5 MPa and the flow velocity 20 m s^{-1}. Depending on the component width (12 to 24 mm) and the resulting cooling channel diameter (8 to 20 mm) this results in heat transfer coefficients ranging from 139 to 116 W $m^{-2}K^{-1}$ according to the Eupiter code [48]. Thermal loads to the W tile were applied in stepwise manner: the initial temperature is set to 700°C, assuming that the FGM is deposited on a bulk W piece and then is joined to a bulk Eurofer counter part by hot pressing at 700°C. This last step of production is assumed to release all formerly introduced residual stresses from FGM production. Subsequent load steps (LS) are carried out as follows:

LS1 component is homogeneously cooled to 20°C
LS2 cooling is activated, the component homogeneously heated to 200°C
LS3 a heat load is applied to the top surface of the W piece while the cooling is active
LS4 when a steady-state heat distribution in the component is achieved within LS3, the heat load is deactivated, resulting in cooling of the component to 200°C
LS5 and LS6 repetition of LS3 and LS4

With respect to the parameter studies, the influence of heat loads from 2 to 4 MW m^{-2} was investigated. In the second operational phase of DEMO heat loads up to 5 MW m^{-2} are expected [40], particularly occurring at highly loaded FW areas, e.g. the upper blanket modules [49]. The temperature, stress and accumulated plastic strain distributions within the component were selected for evaluation of the results.

2.2. *FGM modelling*

In order to model a virtually ideal FGM, a fine mesh was applied exhibiting small quadratic elements (0.01 x 0.01 mm^2) within the FGM part. Based on that, realization of the FGM was achieved applying position-sensitive material properties to each element of the geometry individually. Taking a linear grading of the volumetric Eurofer/tungsten composition, $V_W/(V_W + V_{Fe})$, within the limits of the FGM into account, the corresponding material properties progress in a specific manner over the FGM height depending on the interpolation model that is applied for each property. Where more than one of the interpolation models given subsequently seemed applicable, the most conservative with respect to applicability of the FGM in the FW was selected.

According to Progelhof [50], e.g. the series model, the parallel model and the geometric model are well-established formulae to calculate the temperature sensitive thermal conductivity $\lambda(V_W, T)$ of a composite material from the base materials

Table 1: Tungsten properties used for the FE simulation [44, 45].

Temperature	Young's modulus	Poisson number	Yield stress	Coeff. of thermal expansion	Th. cond.	Heat capacity	Density
°C	GPa	-	MPa	10^{-6} K^{-1}	W (mK)$^{-1}$	J (kgK)$^{-1}$	g cm^{-3}
20	397.9	0.3	1360.46	4.4	161.53	131.45	19.3
200	397.3	0.3	1154.17	4.4	149.34	135.2	19.3
400	394.5	0.3	947.47	4.4	137.79	139.36	19.3
600	389.5	0.3	746.79	4.4	128.14	143.29	19.3
700	386.2	0.3	681.67	4.4	123.96	145.28	19.3
900	378.0	0.3	531.74	4.4	116.76	149.39	19.3
950	375.6	0.3	497.57	4.4			19.3
1000	373.1	0.3	464.69	4.4	113.7	151.56	19.3
1050	370.4	0.3	433.09	4.4	109.2	152.6	19.3

Table 2: Eurofer properties, representing the class of RAFM steels, used for the FE simulation [44, 45].

Temperature	Young's modulus	Poisson number	Yield stress	Coeff. of thermal expansion	Th. cond.	Heat capacity	Density
°C	GPa	-	MPa	10^{-6} K^{-1}	W (mK)$^{-1}$	J (kgK)$^{-1}$	g cm^{-3}
20	217.3	0.3	545.67	12.0	28	472	7.8
200	207.3	0.3	483.62	12.0	30	522	7.8
400	197.1	0.3	446.99	12.0	29	541	7.8
600	177.6	0.3	298.32	12.0	29.7	546	7.8
700	161.0	0.3	134.79	12.0	29.7	549	7.8
900	55.8	0.3	50	12.0	29.7	552	7.8
950	43.9	0.3	36.7	12.0	29.7		7,8
1000	33.8	0.3	29.0	12.0	29.7	553	7.8
1050	30.0	0.3	23.0	12.0	29.7		7.8

properties $\lambda_\mathrm{i}(T)$. The parallel model, given in eq. (1), results in the lowest thermal conductivity of any composition and is thus the most conservative interpolation. In FGMs small volumes of both constituents are usually located next to each other, e.g. resulting from powder metallurgical production. Heat has to pass through both constituents successively overall in consequence further legitimating the applicability of the parallel model.

$$\lambda(V_\mathrm{W}, T) = \left(\frac{1 - V_\mathrm{W}}{\lambda_\mathrm{RAFM}(T)} + \frac{V_\mathrm{W}}{\lambda_\mathrm{W}(T)} \right)^{-1} \tag{1}$$

The FGM density progression $\rho(V_\mathrm{W})$ is described by a linear interpolation of the base densities ρ_i as the FGM can be interpreted as thin layers of identical volumes being stacked one on another while the composition from layer to layer changes in small and identical increments. The corresponding interpolation model is given in eq. (2). In the current simulation, the density is considered temperature insensitive.

$$\rho(V_\mathrm{W}) = V_\mathrm{W} \cdot \rho_\mathrm{W} + (1 - V_\mathrm{W}) \cdot \rho_\mathrm{RAFM} \tag{2}$$

The interpolation of the specific heat capacity $c_p(V_\mathrm{W}, T)$ is based on its physical definition, given in eq. (3), and the assumption that the amount of energy $\Delta Q(T)$ required to heat a composite of mass m by temperature ΔT equals the amount of energy needed to heat the same mass of individual constituents by the same temperature, eq. (5).

$$c_p(T) = \frac{\Delta Q(T)}{m \cdot \Delta \mathrm{T}} \tag{3}$$

Furthermore, taking the aforementioned density progression into account, the heat capacity can be expressed as given in eq. (5).

$$c_p(V_\mathrm{W}, T) = \frac{c_{p,\mathrm{W}}(T) \cdot m(V_\mathrm{W}) \cdot \Delta \mathrm{T} + c_{p,\mathrm{RAFM}}(T) \cdot m(V_\mathrm{RAFM}) \cdot \Delta \mathrm{T}}{\Delta \mathrm{T} \cdot (m(V_\mathrm{W}) + m(V_\mathrm{RAFM}))} \tag{4}$$

$$= \frac{c_{p,\mathrm{W}}(T) \cdot \rho_\mathrm{W} \cdot V_\mathrm{W} + c_{p,\mathrm{RAFM}}(T) \cdot \rho_\mathrm{RAFM} \cdot (1 - V_\mathrm{W})}{\rho_\mathrm{W} \cdot V_\mathrm{W} + \rho_\mathrm{RAFM} \cdot (1 - V_\mathrm{W})} \tag{5}$$

Mechanically, the model considers thermal, elastic and ideal-plastic strain components. Viscoplastic behaviour (creep), fatigue and transformation induced strains were not taken into account. In order to connect strains and stresses within the FGM accurately, Young's Modulus, E, has to be interpolated over the FGM height. The series model, the parallel model and the Halpin-Tsai model are common approaches to calculate Young's Moduli of composite materials according to Weber [32]. The series model, given in eq. (6), results in the greatest values $\mathrm{E}(V_\mathrm{W})$ over the FGM height, giving high stiffness. Given

a certain yield strength and assuming high stiffness, only little strain can be taken up elastically, potentially resulting in higher plastic deformations when the yield strength is exceeded.

$$\mathrm{E}(V_\mathrm{W}, T) = V_\mathrm{W} \cdot \mathrm{E}_\mathrm{W}(T) + (1 - V_\mathrm{W}) \cdot \mathrm{E}_\mathrm{RAFM}(T) \quad (6)$$

In order to account for thermal strains correctly, the thermal coefficient of expansion $\alpha(T)$ has to be interpolated over the FGM height. Viable solutions are the series model, the Turner model and the Kerner model [32]. As the aim of an FGM is to reduce thermally induced stresses, the model whose second differential $\partial^2/\partial V_\mathrm{W}^2$ of the $\alpha(V_\mathrm{W}, T)$ progression yields extreme values at any arbitrary height V_W of the FGM is most conservative because this indicates a locally great difference of thermal expansion coefficients of neighbouring layers. No extreme values are present for any of the considered models and hence the simplest, namely the series model given in eq. (7), was selected for the simulation.

$$\alpha(V_\mathrm{W}, T) = V_\mathrm{W} \cdot \alpha_\mathrm{W}(T) + (1 - V_\mathrm{W}) \cdot \alpha_\mathrm{RAFM}(T). \quad (7)$$

Upon exceeding a critical yield stress, plastic deformation has to be taken into account, too. In the present work the yield stress σ_YS is calculated based on the von Mises yield criterion. In contrast to the Tresca or the Rankine criteria, the von Mises yield criterion applies for a great range of material behaviour from ductile deformation to brittle failure, both of which have to be taken into account for the Eurofer rich and the W rich end of the FGM at high and low temperatures, respectively. The description of the yield stress progression over the FGM height $\sigma_\mathrm{YS}(V_\mathrm{W}, T)$ is challenging because the yield stress strongly depends on the interface adhesion strengths of particles within powder metallurgically manufactured composites. To date no reliable experimental results, nor models for the investigated system exist. The yielding of dual phase steels was described by Petit-Grostabussiat using a theoretically derived solution that may also be applicable to the description of composites based on its origin [51]. The model seems suitable for very homogeneous micro structures only, however. It outputs a minimum yield strength for the FGM layer in the range of 15 to 30 vol.% W (due to local stress intensities) that does neither consider any phase distribution morphology, nor the quality of interfaces. Lacking these considerations, a simpler linear interpolation of the yield stress over the FGM, eq. (8), may equally well be used. This is only a rough estimation and assumes strong interface bonding.

$$\sigma_\mathrm{YS}(V_\mathrm{W}, T) = V_\mathrm{W} \cdot \sigma_\mathrm{YS,W}(T) + (1 - V_\mathrm{W}) \cdot \sigma_\mathrm{YS,RAFM}(T) \quad (8)$$

For the consideration of plastic deformation, a hardening model should be taken into account. Kinematic hardening respects cyclic loads that potentially cause the Bauschinger effect and fatigue. The model is best suited for rather small deformations, whereas isotropic hardening is suited for greater deformations but neglects load orientations. Since neither a properly suited hardening model, nor appropriate strain hardening exponents for the different layers of the Eurofer/W FGM exist, the simplest model, ideal-plastic behaviour, is assumed to represent the FGM plasticity. Using this model, strain controlled deformation yields lower stresses compared to reality (which should be taken into account for evaluation of the stress results), but stress controlled loading yields infinite plastic strain with the used ideal-plastic material behaviour when the yield criterion is fulfilled. Based on strain controlled plasticity, the accumulated equivalent plastic deformation is considered an appropriate damage indicator.

Potentially relevant effects like plastic deformation (losses) due to the reversible α-γ transition of RAFM steels, creep (as suggested in [35]), recovery, neutron damage and thermo shock loads due to plasma instabilities were not taken into account at the present stage.

3. Results and discussion

In a first part of the present work, a geometry of medium size (16 mm width) with respect to the applied limits, loaded by 4 MW m^{-2}, was modelled and examined in detail to understand critical loads. The model contains a 1 mm thick FGM, which exhibits 100 sublayers and is thus considered quasi-linearly graded. A detailed temperature, macrostress and plastic strain analysis is conducted for the given model to understand which properties limit the component's performance over its life time. The results are then compared to a component model with direct Eurofer-W joint. Although the hot pressing of a direct Eurofer-W joint requires higher bonding temperatures than 700°C, the initial stress free temperature was not modified for the direct joint model for the sake of better comparability.

The gained knowledge was then used to perform parametric studies reducing the quantity of sublayers within the FGM from 100 to 1, varying the FGM thickness from 0.3 to 3 mm and modifying the component size from 12 to 24 mm width, each with focus on the previously identified performance limits.

3.1. Detailed analysis

Based on the load steps, described in section 2.1, temperature, stress and plastic strain fields establish across the component. The development of these fields over the load steps is described collectively in the following. With regard to this, fig. 2 depicts the load step progression of a) the min and max temperature within the component and within the FGM in particular, b) min and max von Mises stresses within the component and the FGM, c) the max equivalent plastic deformations, d) - f) the min and max stress components σ_{xx}, σ_{yy} and σ_{xy}.

3.1.1. LS1 - cooling from hot pressing

According to fig. 2 a) the temperature decreases homogeneously within the component, which is indicated by overlapping $\mathrm{T_{min}}$ and $\mathrm{T_{max}}$ progressions. Due to the material mix in the test component, temperature changes cause stresses that reach an overall maximum for all stress components at the end of LS1 as can be seen in figs. 2 d) - f), and consequently also for the von Mises stress, fig. 2 b). The min and max values of all stress components within the FGM part coincide with the min and max values of the stresses in the entire component, revealing

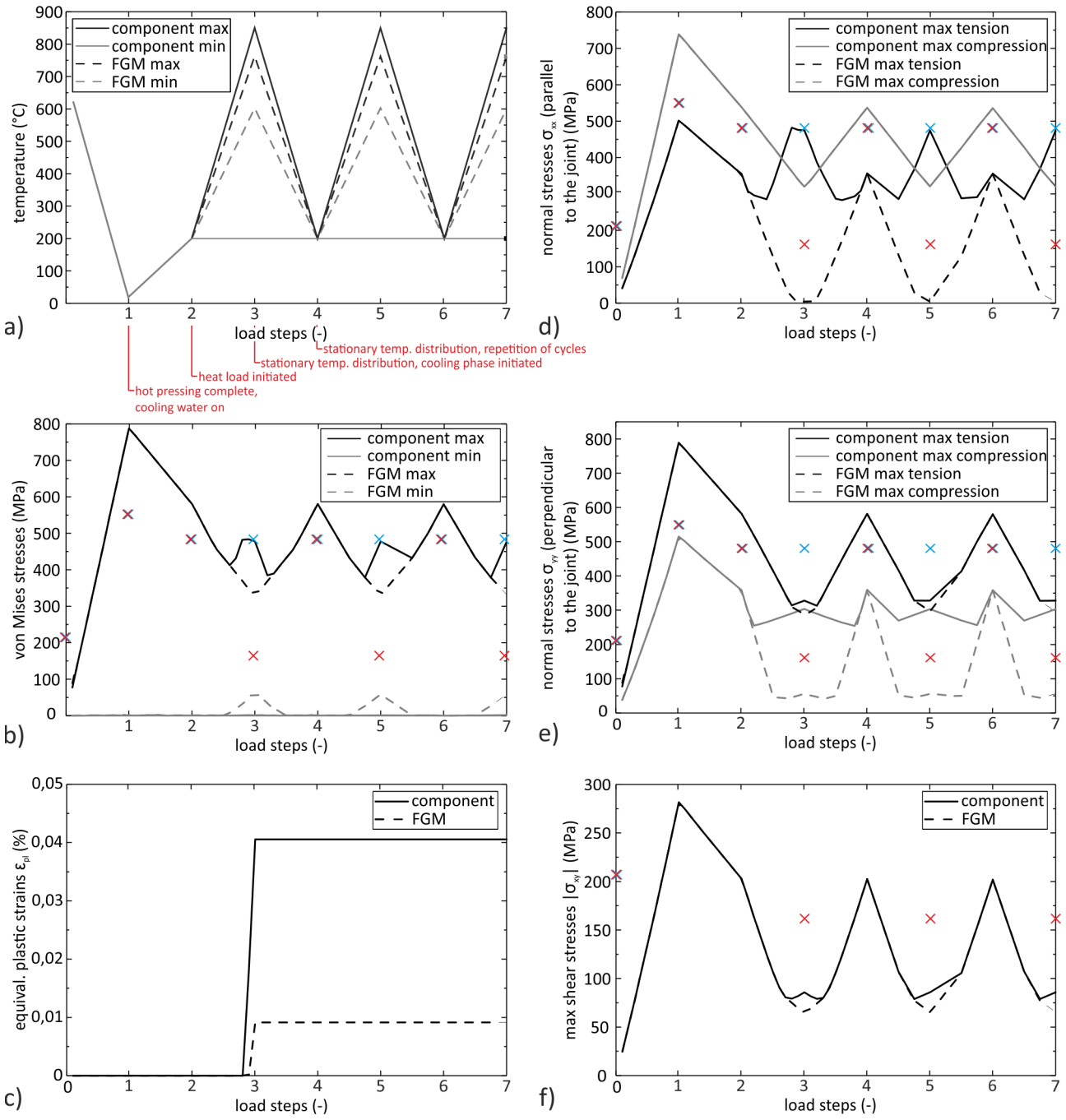

Figure 2: Progressions of temperature, stresses and plastic strains versus load steps. a) temperature minima and maxima within the entire test component and within the FGM in particular, b) minima and maxima of von Mises stresses, c) maxima of the equivalent plastic strains, d) maxima of the tensile and compressive stresses parallel to the joint, σ_{xx}, e) maxima of the tensile and compressive stresses perpendicular to the joint, σ_{yy}, f) max values of the shear stresses, σ_{xy}. The stress progressions additionally show the temperature dependent yield strengths of Eurofer at the lowest temperature (blue crosses) and the highest temperature of any LS (red crosses) in the component.

that the stress maxima are contained within the FGM. Here, compressive stresses parallel to the joint, σ_{xx}, are greater than tensile stresses of the same orientation, fig. 2 d). Furthermore, the former are greatest at the W rich end of the FGM, given that the max value of 739 MPa exceeds the yield strength of Eurofer (approx. 550 MPa) while no plastic deformation takes place in the test component until the end of LS1 according to fig. 2 c). Tensile stress maxima σ_{xx} are always lower than the Eurofer yield strength and have to be located at the steel rich end of the FGM in order to balance the overall stress profile. Regarding stresses perpendicular to the joint, σ_{yy}, the tensile stress max reaches 789 MPa and must be located in the W rich FGM area to accord with non-existent plastification, whereas compressive stresses are limited to 515 MPa. Shear stresses can only be localised with the aid of contour plots. Exemplary contour plots of all mentioned stress components at the end of LS1 are depicted in fig. 3.

The plots of fig. 3 confirm the aforementioned results and furthermore indicate a compact circular shear stress field close to the component's vertical edges. The field results from the normal stress distributions that feature very localised σ_{yy} maxima at the component's vertical edges and greater, elongated σ_{xx} stress fields propagating along the component's joints. Since σ_{xx} tensile stresses mainly propagate into the Eurofer component and σ_{xx} compression stresses into the W part, the centre of the FGM is nearly free of stresses. This situation also becomes evident from the von Mises stress distribution additionally shown in fig. 3. In the literature, often times solely von Mises stresses are investigated in order to assess the stress induced failure risk of fusion relevant components. With respect to the components manufacture, however, the formation of von Mises stresses has to be taken into account, too, as e.g. compressive stresses are less detrimental at interfaces and cracks than tensile stresses. For the given case, von Mises stresses at the centre of the W-FGM joint pose a less significant threat compared to the localized von Mises stress max at the outer edge of the W-FGM joint. The latter has to be considered critically at all following parameter studies, because it can easily induce cracks at the potentially weak joint.

3.1.2. LS2 - transition from production to application

LS2 describes the transition from producing the component to its application in a reactor. The component is homogeneously heated to 200°C, i.e. brought closer to the original stress free state. Since no plastic deformations were introduced during LS1, the stress state does not change qualitatively during LS2, only the max values decrease as can be seen in fig. 2 b) and d) - f).

3.1.3. LS3 - application of the first reactor-relevant heat load

The application of heat loads is modelled to occur in linearly increasing manner, aiming for numerical stability. In consequence, the max temperature progression behaves alike, resulting in approximately 850°C in the W part and 763°C in the FGM when the full heat load of 4 MW m^{-2} is established, as shown in fig. 2 a). While the reached temperatures do not pose any risk to the W part, the FGM is heated close to the α-γ transition temperature of the contained Eurofer (approximately 820°C [52]) that represents its upper tolerable temperature. Taking engineering safety factors into account, at the given load a leaner structure may be necessary for actual FW components that removes heat more effectively. The temperature contour plot of the end of LS3, depicted in fig. 4, exhibits isotherms that follow the shape of the cooling channel, causing the max temperature to be located at the component's outer edges. It may be noted here, that rectangular cooling channels, as anticipated for real FW components of DEMO and modelled by Igitkhanov and Emmerich [39, 41], may yield lower max temperatures.

The stress distribution develops in complex manner during LS3. According to fig. 2 d) the global σ_{xx} compression stress max is contained in the FGM part (coinciding progressions). With increasing temperature, σ_{xx} compressive and tensile stresses in the FGM are reduced so that the part is virtually not experiencing σ_{xx} tensile stresses and 320 MPa compression stresses only. Particularly interfaces, which will be present in the FGM joint, are more sensitive to tensile than to compression stresses, following that the described stress development is beneficial. While the σ_{xx} compressive stress max within the entire component behaves alike, the corresponding tensile stress max progression differs from that behaviour. After slowly decreasing during LS3 it spontaneously increases, only being limited because the Eurofer yield strength is reached, and then progresses at a constant level. Fig. 5 a) shows the stress distribution contour plots at the end of LS3 and puts the mentioned stress development into picture. Due to the inhomogeneous temperature profile a new σ_{xx} stress field establishes on top of the cooling structure that exceeds the σ_{xx} stresses within the FGM. The counter-developing stress fields cause a shift of the global σ_{xx} max and explain the σ_{xx} progression during LS3. The new σ_{xx} field is a result of the circular cooling pipe that is accompanied by a fairly high stress intensity factor, being responsible for reaching the 200°C yield strength of Eurofer that occurs at this location. A rectangular cooling channel, used in the FW of DEMO, may ease the stress profile, re-distributing stresses to a lower max.

Stresses perpendicular to the joint, σ_{yy}, behave similar to σ_{xx} tensile stresses. While the σ_{yy} compressive and tensile stress maxima within the FGM decrease throughout LS3, the compressive stress max of the entire component first behaves likewise but then slowly re-increases from half of the load step, later being followed by the tensile stress max σ_{yy}. Compressive and tensile stresses reach 303 and 328 MPa eventually. As can be seen in fig. 5 b) again a new σ_{yy} tensile stress field is established right and left of the cooling channel. The shift of the max σ_{yy} tensile stress location is even more important than the shift of the σ_{xx} max because severe σ_{yy} stresses are re-located from the potentially weak W-FGM interface to the homogeneous and ductile cooling structure, reducing the failure risk at reactor-relevant heat loads. As a consequence of re-increasing σ_{xx} and σ_{yy} stresses, the global shear stresses behave likewise. Fig. 5 c) shows the shear stress distribution at the end of LS3. The max is located at the circumference of the cooling structure.

Linking the previously mentioned stress behaviours to the

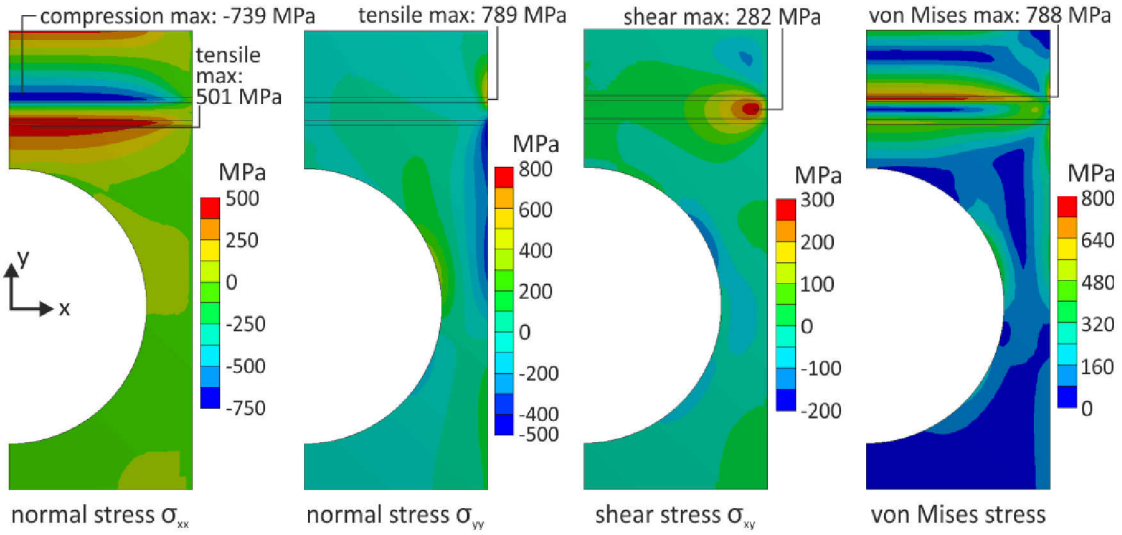

Figure 3: Contour plots of the stress components' distributions at room temperature after hot pressing. Only the right half of the symmetric test component is depicted.

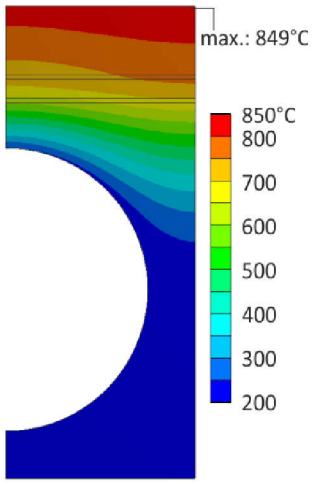

Figure 4: Temperature contour plot at 4 MW m^{-2} heat load. Only the right half of the symmetric test component is depicted.

global von Mises stress max progression, it becomes evident that the LS3 peak in fig. 2 b) is related to σ_{xx} tensile stresses. The LS1 peak, in contrast, was related to σ_{yy} tensile stresses. With regard to failure, this difference has to be taken into account. Not only does the LS3 peak refer to a less critical position (the ductile cooling structure) than the LS1 peak (the W-FGM joint), but also has the stress component causing the LS1 peak a critical orientation with respect to the joint. Following the explained stress distributions, macrostresses do not seem to pose a risk of spontaneous failure of the component during reactor-relevant heat loads.

Besides macrostresses, plastic strain, ε, has to be evaluated with respect to failure risk of the component. As figs. 2 c) and d) indicate, the previously mentioned constant progression of the global σ_{xx} tensile stress max is accompanied by plastic deformation. It reaches 0.04 % globally. In accordance with the stress distribution, given in fig. 5 a), fig. 6 a) indicates that the max plastic deformation at the end of LS3 occurs right above the cooling channel. Since the presented model does not take hardening into account, the question whether plastic deformation increases cyclically and results in fatigue damage in the test component remains open. Apart from the global max plastic field, a second smaller field appears at the FGM-Eurofer interface. It is limited to 0.009 % and yet during LS3 it can be described as point deformation (cf. fig. 6 b)). In a subsequent heat load (LS5), however, the plastic field increases in size and then stabilizes as shown in figs. 6 b) and c). The max value always remains unchanged according to fig. 2 c). Reason for the growth of the local plastic field is given reciprocally by further analysis of the max stresses developments.

3.1.4. LS4 to LS7 - subsequent reactor-relevant heat loads

According to fig. 2 both temperature and max stresses basically show a reproducible, cyclic behaviour from the end of the first reactor-relevant heat load. Only at the end of the second heat load, when the local plastic field at the FGM-Eurofer interface increases, discrepancies are apparent that are to be attributed to the greater plastic deformations above the cooling channel. Since these deformations were caused by high σ_{xx} tensile stresses at elevated temperatures, slight compression stresses are formed in this area during cooling (cf. fig. 2 d), LS4). At the end of the first reactor-relevant heat load they reach 45 MPa. Due to this new compression stress field the σ_{xx} tensile and compression stress maxima at the FGM-Eurofer interface are slightly reduced as compared to the end of LS2. Hence, during the second reactor-relevant heat load the maxima of all stress components change locations a bit earlier compared to the first heat load. The behaviour is especially pronounced for the max σ_{yy} and σ_{xy} stresses (figs. 2 e) and f)). Since plastic deformation above the cooling channel occurred already and no kinematic hardening is considered here, no plateau of the max σ_{xx} tensile stresses establishes during the second heat load (fig. 2 d), LS5). Simultaneously, max σ_{yy} and σ_{xy} stresses de-

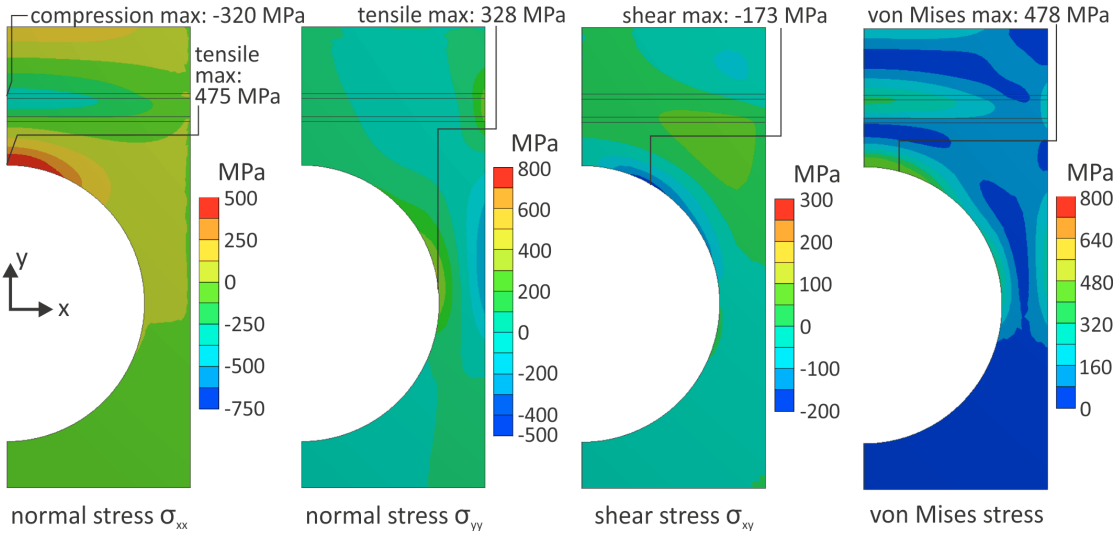

Figure 5: Contour plots of the stress components' distributions at 4 MW m^{-2} heat load. Only the right half of the symmetric test component is depicted.

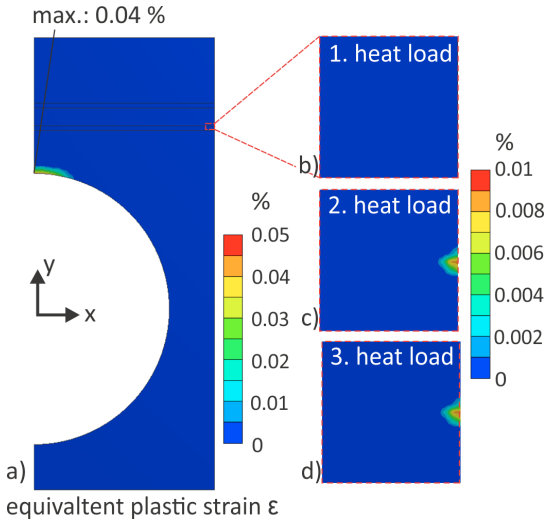

Figure 6: Contour plots of the equivalent plastic strain distribution within an FGM-featured test component at 4 MW m^{-2} heat load. Only the right half of the symmetric component is depicted.

crease less than during LS4 because the plasticised area above the cooling channel yields an earlier increase of σ_{xx} stresses, which also requires the other stress components to increase to preserve the global stress equilibrium. With this development, local plastic deformations at the FGM-Eurofer interface increase in size eventually.

For additional loads, the component shows no other behaviour than the mentioned with the applied model.

3.2. Component with direct Eurofer-W joint

Although high heat loads were assumed, modelling of an FGM-featured test component reveals limited plastic deformation within the Eurofer-W transition as described in the previous section. A matching model that exhibits the same boundary conditions as the previously described, but does not have the FGM part, was analysed to put the calculated critical loads (T, σ, ε) into perspective. Geometries are the same, only the height of the direct Eurofer-W joint component is one millimetre less with the FGM part being removed.

The max temperature, max stresses, and max plastic strain results, present in the direct Eurofer-W joint zone and in the FGM zone, respectively, are comparatively depicted in fig. 7. Dashed lines are the previously described results of the "detailed analysis" section 3.1 and serve as guidance.

Fig. 7 a) confirms an identical cooling after hot pressing and re-heating to 200°C of both models (LS1+2). During reactor-relevant heat loads, the max temperature of the direct Eurofer-W joint component is up to 50 K lower than that of the FGM-featured component, a circumstance that is related to the differing wall thickness between plasma and cooling channel.

In terms of stresses, figs. 7 d) - f) indicate that max values of the direct Eurofer-W joint component exceed the FGM-featured component's max values significantly over almost the entire life cycle. Already at half of the first load step this causes exceedance of the Eurofer 360°C yield strength due to high σ_{yy} tensile stresses. Accompanying equivalent plastic deformations reach 5.5 %, being 600 times greater than max plastic deformations in the FGM-featured component (cf. fig. 7 c)). Moreover, plasticity in the latter only occurs during reactor-relevant heat loads instead of already during production and does not increase during the first three load cycles. In contrast, fig. 7 c) shows further gain of plastic strains in the direct Eurofer-W joint component with LS6. Position of the max plastic strain field after hot pressing and at the end of each of the first three reactor-relevant heat loads is shown in fig. 8. Other than in the FGM-featured component, plastic strain above the cooling channel is negligible compared to the plastification at the Eurofer-W joint. The latter strain field's position matches the local strain max of the FGM-featured component, but reaches deeper into the component along the interface, eventually causing more plastification damage. In accordance with the very small gain of plastification during LS6, the strain field changes only marginally (cf. fig. 8 c) - e)).

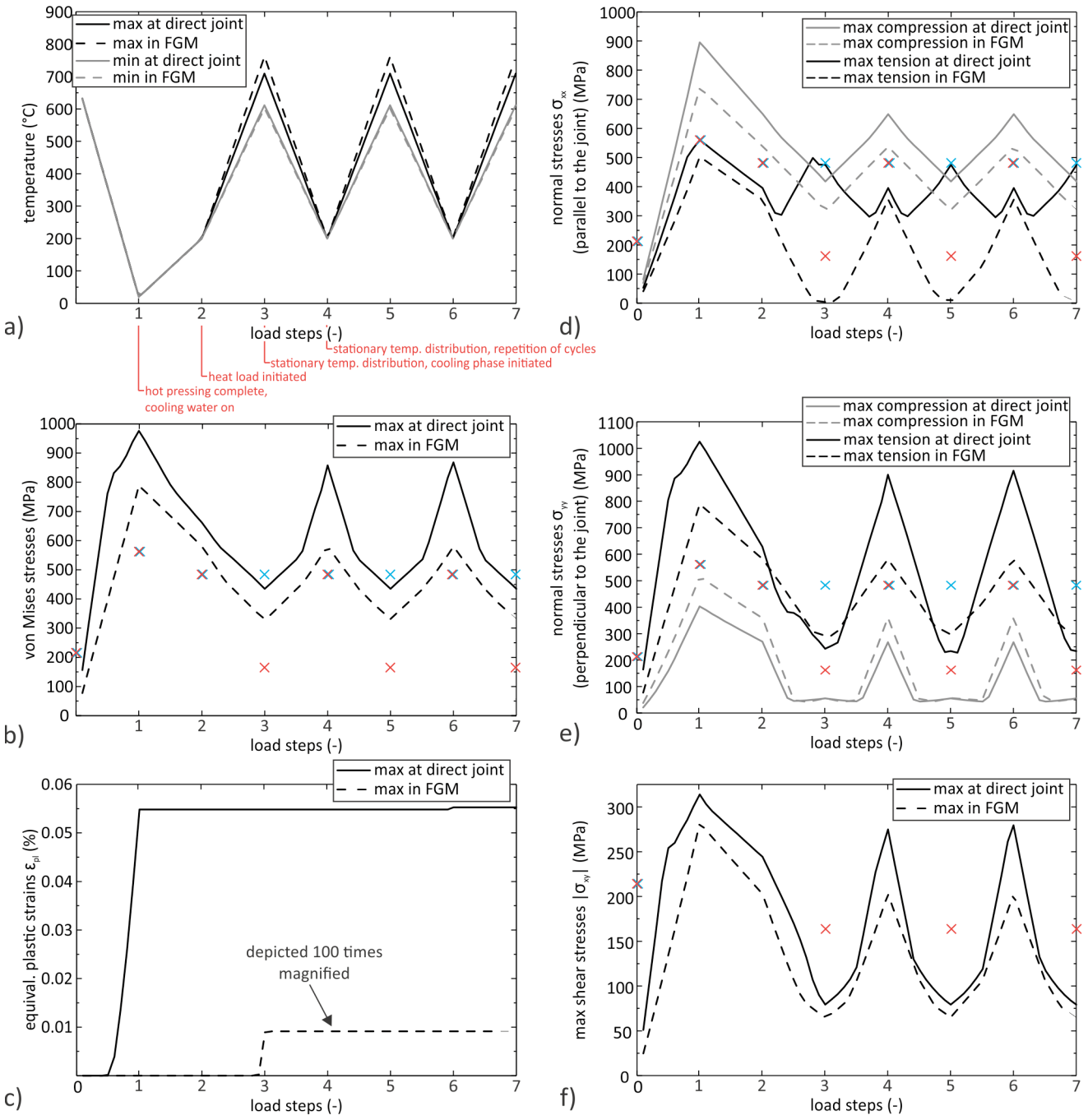

Figure 7: Progressions of temperature, stresses and plastic strains versus load steps, comparatively for test components with FGM and with direct Eurofer-W joint. The values refer to the situation at the joint and in the FGM, respectively. a) temperature minima and maxima, b) minima and maxima of von Mises stresses, c) maxima of the equivalent plastic strains, d) maxima of the tensile and compressive stresses parallel to the joint, σ_{xx}, e) maxima of the tensile and compressive stresses perpendicular to the joint, σ_{yy}, f) max values of the shear stresses, σ_{xy}. The images additionally show the temperature dependent yield strengths of Eurofer at the lowest temperature (blue crosses) and the highest temperature of any LS (red crosses) in the FGM-featured component.

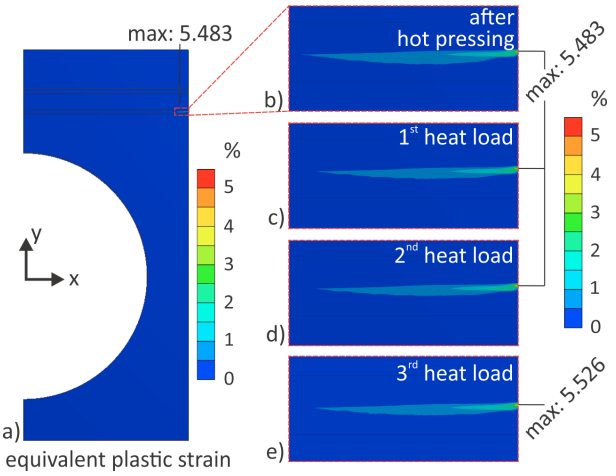

Figure 8: Contour plots of the equivalent plastic strain distribution within a test component without FGM (direct Eurofer-W joint) at 4 MW m^{-2} heat load. Only the right half of the symmetric component is depicted.

In consequence of early plastic deformations of the direct Eurofer-W joint component, in particular max σ_{xx} stresses differ significantly from the FGM-featured component's σ_{xx} stresses as fig. 7 d) reveals. The max σ_{xx} stress progression, inverting at half of LS3, results in high stresses (475 MPa) not only at low but also at high temperatures. This is crucial because the Eurofer part is sensitive to further plastic deformation due to softening. During the plateau-like progression of the max σ_{xx} stresses, the plastic strain field changes in shape (while the max is constant), that is also evident from fig. 8 b) and c). The behaviour causes an increase of all stress components at cooling water temperature, compared to before the first reactor-relevant heat load.

Based on the detailed loads analysis and the comparison of component models with and without FGM, the effect of the implemented FGM is evaluated as beneficial at this stage. No unacceptably high temperatures are reached in the FGM-featured component although high heat loads and a conservative heat conduction model were assumed. Macroscopic plastic deformations within the FGM are limited effectively compared to within the direct Eurofer-W joint. Production-inherent macroscopic stresses however still pose a threat to the test component and possibly to actual FW components. Based on the given analyses, they always should be taken into account in detail.

3.3. FGM parameter study

In the frame of parameter studies, the number of sublayers, the FGM thickness and the component width were successively varied to assess favourable specifications of the FGM. All other boundary conditions remained unchanged as compared to the previously described model. Unless stated specifically, the load step progressions of temperature, stress components and plastic strain do not change qualitatively compared to the detailed analysis. Hence, only crucial states of interest were selected based on damage potentials and analysed. These are

- the max von Mises stresses and equivalent plastic strains at the end of LS1 because after hot pressing stresses are the greatest over the life cycle of a FW component.
- the max temperature within the FGM at the end of LS3 because here temperatures are close to the limiting α-γ transition.
- the max plastic deformation at the end of LS3 because this is when plastic deformations first occur when applying the linearly graded, 1 mm thick FGM.

Each parametric study is analysed based on an integrated evaluation of the named states eventually.

3.3.1. Number of sublayers

Within the detailed analysis of the previous section, the FGM was composed of 100 sublayers that equals a quasi-linear grading. Regarding technical feasibility, fewer, thicker sublayers are preferable as they can be manufactured easier. Based on that idea, the number of sublayers was successively reduced to one. Results of the mentioned states of interest are given in fig. 9 in that a) depicts von Mises stresses and equivalent plastic strains after hot pressing (end of LS1), and b) temperature and plastic strains at the maximum heat load (end of LS3).

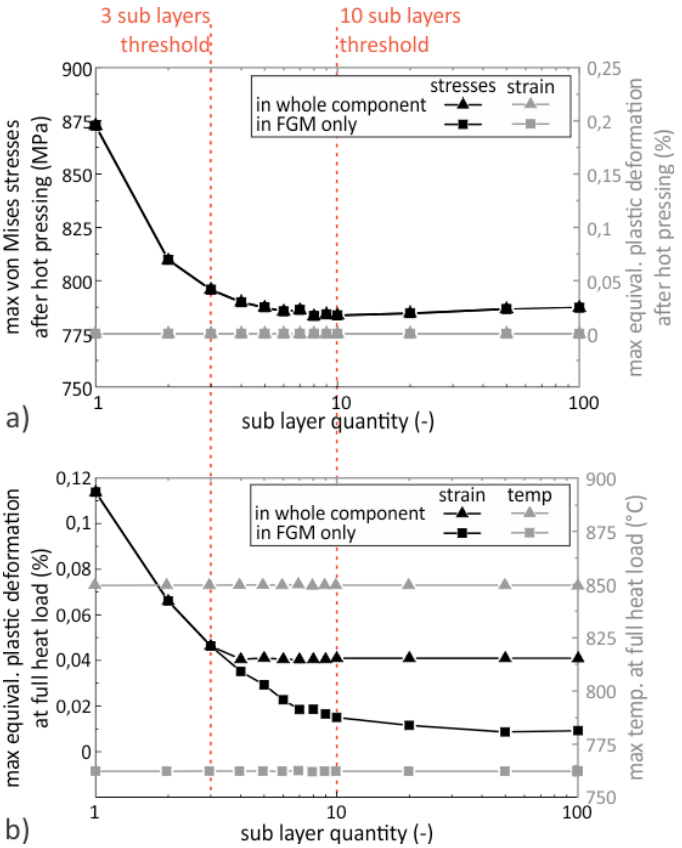

Figure 9: Influence of the number of sublayers of an FGM on a) max von Mises stresses and max equivalent plastic deformation after hot pressing and on b) max equivalent plastic deformation and max temperature at full heat load of 4 MW m^{-2}. FGM thickness: 1 mm, component width: 16 mm.

As for the situation after hot pressing, reducing the number of sublayers by 90 % does not have a detrimental effect on the

stress max according to fig. 9 a). The max von Mises stresses decrease slightly, which may be attributed to lower Young's moduli in the area of the former upper most sublayers that is represented by only one average Young's modulus with reducing the total sublayer quantity to ten. With less than ten sublayers the von Mises stress max increases progressively to 796 MPa (101 % of the stress max for 100 sublayers) when considering three sublayers and to 874 MPa (111 %) with only one sublayer. Reason for that is a less effective redistribution of stresses when the number of sublayers is reduced (especially below three), causing stress concentrations at the sublayers' interfaces. The highest concentration is again located at the W-FGM interface as apparent from fig. 10.

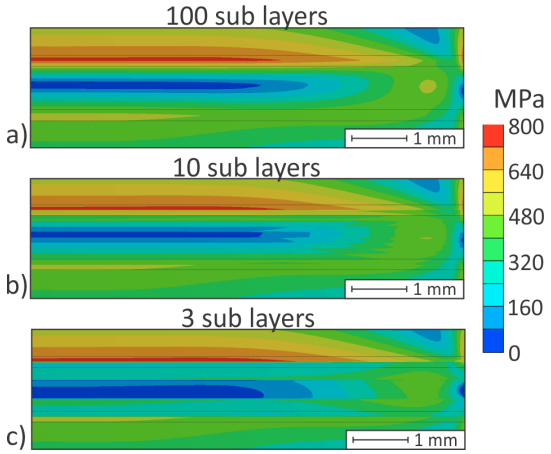

Figure 10: Contour plots of the von Mises stress distribution within the FGM for a) 100, b) 10 and c) 3 sublayers after hot pressing.

Macroscopic plastic deformations after hot pressing are inexistent for any number of sublayers in the used model according to fig. 9 a). Likewise, the quantity of sublayers has no influence on the max temperature of the component during reactor-relevant heat loads, fig. 9 b). This is reasonable as the overall thermal conductivity of the FGM remains unchanged with a modification of the sublayer quantity. In contrast, the influence of sublayers on the plastification max during reactor-relevant heat loads has to be taken into account. In both the whole component and particularly the FGM, the max plastic deformation is almost constant when reducing the number of sublayers from 100 to ten. Again, less than ten sublayers cause a progressive increase of plastic strains within the FGM. With less than four sublayers local plastification at the FGM-Eurofer interface exceeds the plastic strain max above the cooling channel. The global max changes position towards the FGM and eventually a collective increase to $\varepsilon > 0.11$ % plastification in the entire component with only one sublayer is caused.

Based on the shown load vs. sublayer quantity progressions, a three-sublayers-FGM seems to be an appropriate compromise about performance and manufacturability. The strong increase of stresses with less than three sublayers does not justify a slightly easier production, especially as the von Mises stresses relate to σ_{yy} stresses at the weak edge of the W-FGM interface. The reduction of sublayer quantity to three does furthermore not affect the max temperature and causes only a small increase of plastic strains.

3.3.2. *FGM thickness*

While a thicker FGM interlayer may redistribute macrostresses more effectively compared to a thinner one, the accompanied increase of wall thickness may cause an intolerable rise of temperature (and neutron capture in an actual FW part). For a given component size and heat load, there is hence an ideal FGM thickness that has to be identified. The thickness subsequently determines potential FGM production methods such as thin film deposition or powder metallurgy based processes.

Results of a parameter study that focusses on an FGM thickness from 0.3 to 3 mm are depicted in fig. 11 in analogous manner as in the previous subsection. The results of the direct Eurofer-W joint test component are indicated by thickness "0.0". Based on the gained results of the previous section, the FGMs were modelled containing three sublayers to obtain conservative and technologically relevant results. Besides 4 MW m^{-2} heat load, 2 MW m^{-2} were modelled to picture more loading scenarios. Contour plots are not depicted because T, σ, and ϵ distributions correspond to the ones already given, only stretched or compressed vertically.

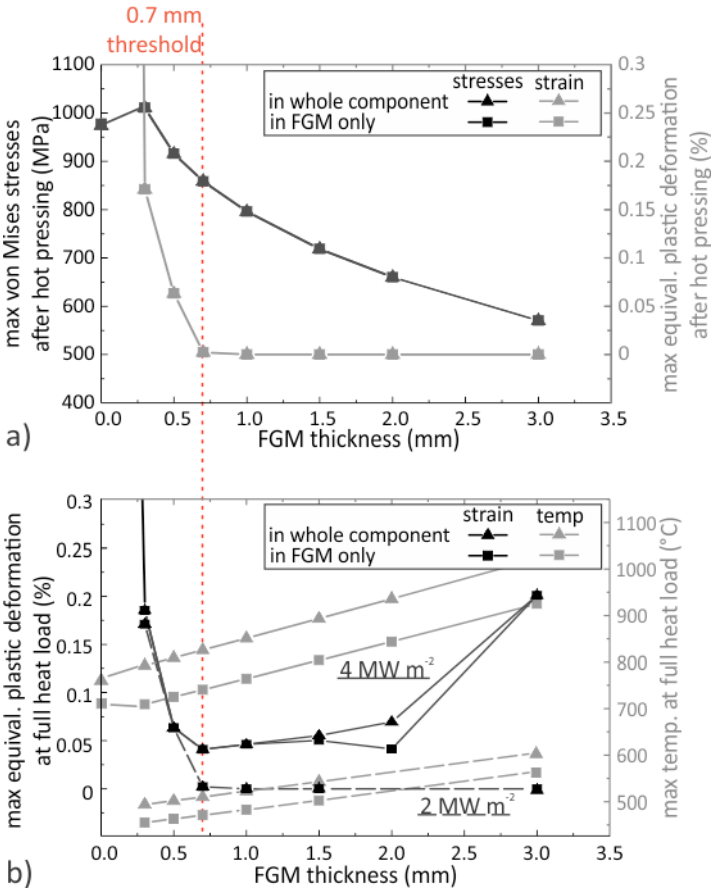

Figure 11: Influence of the FGM thickness on a) max von Mises stresses and max equivalent plastic deformation after hot pressing and on b) max equivalent plastic deformation and max temperature at full heat load of 2 and 4 MW m^{-2}. Component width: 16 mm, sublayer quantity: 3.

For the state after hot pressing, the von Mises stress max decreases monotonically with increasing FGM thickness according to fig. 11 a). The highest value of approx. 1 GPa is obtained with a 0.3 mm thick FGM, whereas an increase of thickness to 3 mm causes a 40 % stress drop. Only the direct Eurofer-W joint component (thickness 0 mm) deviates from the stress propagation behaviour, showing a low stress max of approximately 775 MPa. This however, is only possible due to plastification already having occurred at this stage, as described in the "component with direct Eurofer-W joint" section 3.2 and apparent from the plastic strain progression of fig. 11 a). Compared to that, plastification in the presence of an FGM is strongly reduced even with thin interlayers of 0.3 mm thickness. FGMs thicker than 0.7 mm may even eliminate all macroscopic plastic strains during cooling from hot pressing. For reactor-relevant heat loads, the max temperature within the component and the FGM in particular increases linearly with FGM thickness, fig. 11 b). The global max temperature reaches 1050°C for 4 MW m^{-2} heat load and 3 mm FGM thickness. It is located in the W part, whose lower and upper temperature limits are 550 and 1300°C (not taking neutron irradiation induced embrittlement into account) [40]. The FGM reaches approximately 930°C and thus exceeds the α-γ-transition temperature of the contained Eurofer by about 110 K [52]. In order to remain below this threshold in the FGM, the FGM thickness has to be limited to 1.5 mm for 4 MW m^{-2} heat load. This upper thickness limit is in line with the analysis results of plastic deformations taking place during reactor-relevant heat loads, also shown in fig. 11 b). While the max plastification with FGMs thinner than 0.7 mm and heat loads of 4 MW m^{-2} establish during the cooling stage after hot pressing, FGMs thicker than 1.5 mm also yield significant plastic deformation that develop upon application of the first reactor-like heat load. In total, for 4 MW m^{-2} heat load the lower and upper FGM thickness limits are 0.7 and 1.5 mm based on a stress, temperature and strain analysis. A thickness of 1.0 mm, seeming to be a good compromise, is suggested for production of actual test component, indicating the necessity of powder metallurgical production routes.

A lower heat load of 2 MW m^{-2} does not pose a risk to exceed upper temperature limits of Eurofer or W, or to cause plastic deformation other than during production for any FGM thickness. In the tungsten part, however, the temperature dips below the lower, DBTT-related limit of 550°C when implementing FGMs thinner than approximately 2 mm in the suggested design. Given this, thick FGMs of at least 2 mm are favourable for low heat loads, which is in accordance with the max von Mises stresses, fig. 11 a), but disagrees with an upper thickness limit of 1.5 mm for a heat load of 4 MW m^{-2}. It can, hence, be derived that the FGM thickness has to be adapted to the expected heat load.

3.3.3. Component width

Since the FGM reduces macrostresses and strains, the positive impact is to be evaluated with respect to the component size. In the framework of a parameter study, the width of the test component is varied from 12 to 24 mm. While the thickness of the tungsten part and the FGM part are kept constant (3 and 1 mm), the height of the Eurofer piece and diameter of the cooling channel are modified accordingly, maintaining a quadratic outer cross section and 2 mm leanest wall thickness. Along with that, the heat transfer coefficient of the cooling structure is modified based on results of the EUPITER code. Like in the previous sections, the FGM consists of three sublayers.

Max von Mises stresses and equivalent plastic strains after hot pressing of components of different sizes are depicted in fig. 12 a). While plastic strains are always zero, except for in the largest component of 24 mm width, von Mises stresses decrease with increasing component size up to 20 mm width. In greater test components von Mises stresses increase again, which may be explained by the stress components causing the von Mises stresses. As was explained in the detailed analysis section, max von Mises stresses mainly base on the max σ_{xx} compression stresses in the W part and on the max σ_{yy} tensile stresses at outer regions of the W-FGM interface with σ_{yy} stresses being slightly dominant. Increasing the component width, the ratio of Eurofer wall thickness to component width shrinks, being accompanied by a declining σ_{yy} tensile stress max. Simultaneously, the σ_{xx} tensile and compression maxima above the cooling channel and the FGM, respectively, grow. For components up to 20 mm width these opposing trends cause a decrease of the equivalent stress max. When the width exceeds 20 mm, σ_{xx} compressive stresses become dominant, causing a sudden increase of the von Mises stress max in the 22 mm wide component as apparent from fig. 12 a). Further enlargement of the component by 2 mm causes the σ_{xx} tensile stress max to exceed the Eurofer 200°C yield strength. Plastification above the cooling structure yields a lower σ_{xx} compression stress max above the FGM, eventually, resulting in lower von Mises stresses again. In terms of production induced loads, a suitable component may be 20 mm wide.

Considering the temperature max, the mentioned width limit may be confirmed for heat loads as high as 4 MW m^{-2} according to fig. 12 b). Only in components wider than 20 mm, intolerable temperatures are reached in the FGM part. The upper temperature limit of W is never exceeded for any of the analysed component sizes. Lower heat loads of 3 and 2 MW m^{-2} do not cause the temperature to exceed the upper tolerable limit of neither tungsten nor Eurofer for any of the examined test component widths. The lower temperature limit of tungsten, however, is gone below for low heat loads of 2 MW m^{-2} and small components (< 20 mm). A thicker FGM in this case helps to increase the temperature above the threshold. Although a thicker FGM is not necessary regarding plastic deformations, as these are effectively suppressed already by a 1 mm thick FGM at 3 and 2 MW m^{-2} heat load (cf. fig. 12 c)), a slightly thicker FGM may reduce the failure risk by keeping the W part in the ductile temperature window while maintaining zero macroscopic plastic deformation. In contrast, at reactor-relevant heat loads of 4 MW m^{-2}, plastification has to be taken into account for components wider than 14 mm. Based on the results of the "detailed analysis" section 3.1, the equivalent plastic deformation of components as wide as 16 mm seem tolerable, while greater components suffer from too much deformation damage.

Eventually, the suggested component width depends on the

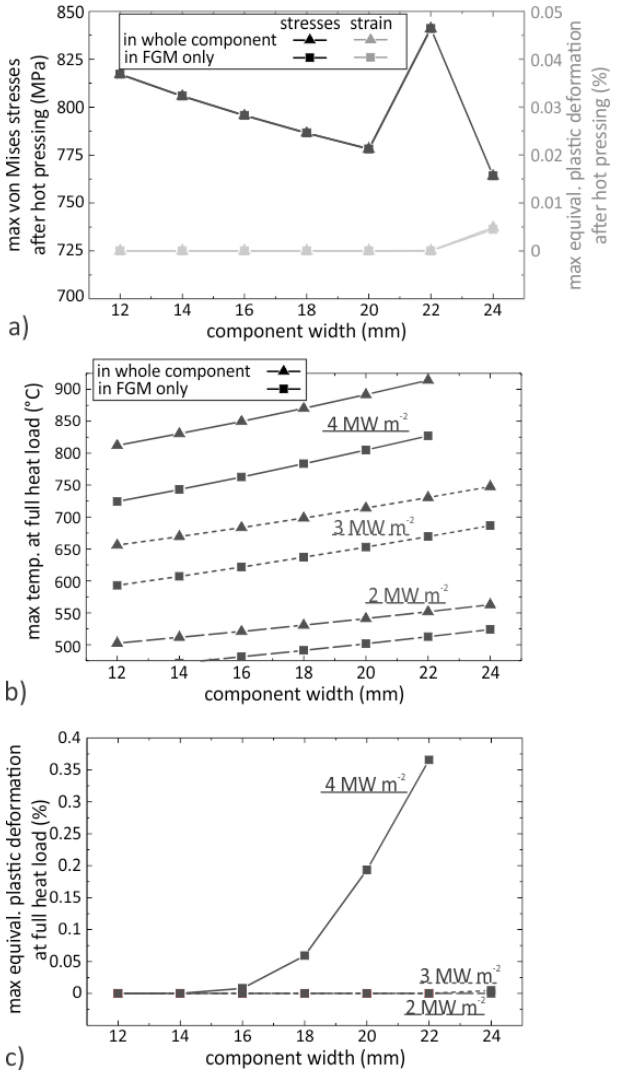

Figure 12: Influence of the component width on a) max von Mises stresses and max equivalent plastic deformation after hot pressing and on b) and c) max temperature and max equivalent plastic deformation at full heat load of 2, 3 and 4 MW m^{-2}. Sublayer quantity: 3, FGM thickness: 1 mm.

expected load again. Greater components of 20 mm width, exhibiting thicker FGMs are preferred for loads $\leq$ 3 MW m^{-2}, whereas smaller components of 16 mm width are suitable to withstand high loads of 4 MW m^{-2}.

4. Conclusion

In the present work, Eurofer-W test components with stress relieving functionally graded material (FGM) interlayers are studied. First, existing mathematical models for the calculation of FGM properties were presented and evaluated. Conservative models were selected and implemented in a subsequently suggested FE model of a test component. A detailed loads analysis and comparison with an equivalent model with no stress relieving interlayer revealed the following:

1. Production related loads in Eurofer/W components may not be neglected.
2. Describing the stress state requires the actual stress components to be taken into account, since materials and geometries are sensitive to loading orientations. Considering von Mises stresses only does not pay attention to specific weaknesses of a component.
3. Critical loads were identified to be (i) σ_{yy} tensile stresses at the outer edge of the W-FGM interface after manufacture, (ii) the temperature within the FGM during reactor-relevant heat loads and (iii) the equivalent plastic deformation during reactor-relevant heat loads.
4. Macroscopic plastic deformations within the Eurofer-W joint of the modelled component may be 600 times lower when implementing a 1 mm thick FGM compared to a component with direct Eurofer-W joint.

In subsequent parametric analyses of the model, several properties were modified, examining production and application based limits of an FGM-featured test component. The study concluded that

1. Based only on performance, an FGM is ideally composed of 10 sublayers. More sublayers do not yield better results. Considering also simple manufacture of the FGM, three layers are a good compromise that reduces the quantity of differing layers to produce and still keeps plastic deformations in the component at a minimum.
2. The optimum FGM thickness depends on the thermal loads to be expected. For the given model and heat loads of 4 MW m^{-2} the FGM thickness may range from 0.7 to 1.5 mm. A thickness of 1.0 mm, lying well within this margin, is suggested for production and indicates the necessity of powder metallurgical FGM production routes. For lower heat loads, the stress-redistributing performance improves with thicker FGMs of up to 3 mm due to lower fabrication-related stresses.
3. The tolerable width of a test component also depends on the expected thermal loads. Due to manufacture related stresses, the component width must not exceed 20 mm. While this size is suited for heat loads up tp 3 MW m^{-2}, heat loads of 4 MW m^{-2} require the component to be max 16 mm wide due to heat load related plastic deformation.

The gained knowledge may help to understand the stress-strain evolution in more complex actual FW components of DEMO, being larger than the suggested test component, exhibiting curvature and numerous cooling channels.

Appendix A. Acknowledgements

This work has been carried out within the framework of the EUROfusion Consortium and has received funding from the Euratom research and training programme 2014-2018 under grant agreement No 633053. The views and opinions expressed herein do not necessarily reflect those of the European Commission. Part of the work was also supported by Czech Science Foundation through grant no. 17-23154S.

Appendix B. References

[1] A. Li-Puma, M. Richou, P. Magaud, M. Missirlian, E. Viscac, V. P. Ridolfini, Potential and limits of water cooled divertor concepts based on monoblock design as possible candidates for a DEMO reactor, Fusion Engineering and Design 88 (2013) 1836–1843.

[2] N. P. Taylor, R. Pampin, Activation properties of tungsten as a first wall protection in fusion power plants, Fusion Engineering and Design 81 (2006) 1333–1338.

[3] L. Tan, Y. Katoh, A.-A. Tavassoli, J. Henry, M. Rieth, H. Sakasegawa, H. Tanigawa, Q. Huang, Recent status and improvement of reduced-activation ferritic-martensitic steels for high-temperature service, Journal of Nuclear Materials 479 (2016) 515–523.

[4] J. M. Missiaen, J. J. Raharijaon, A. Antoni, C. Pascal, M. Richou, P. Magaud, Design of a W/steel functionally graded material for plasma facing components of DEMO, Journal of Nuclear Materials 416 (2011) 262–269.

[5] W. W. Basuki, J. Aktaa, Investigation on the diffusion bonding of tungsten and Eurofer97, Journal of Nuclear Materials 417 (2011) 524–527.

[6] W. W. Basuki, J. Aktaa, Diffusion bonding between W and Eurofer97 using V interlayer, Journal of Nuclear Materials 429 (2012) 335–343.

[7] T. Weber, M. Stüber, S. Ulrich, R. Vaßen, W. W. Basuki, J. Lohmiller, W. Sittel, J. Aktaa, Functionally graded vacuum plasma sprayed and magnetron sputtered tungsten/Eurofer97 interlayers for joints in helium-cooled divertor components, Journal of Nuclear Materials 436 (2013) 29–39.

[8] W. W. Basuki, R. Dahm, J. Aktaa, Thermomechanical analysis of diffusion-bonded tungsten/Eurofer97 with a vanadium interlayer, Journal of Nuclear Materials 435 (2014) 635–639.

[9] W. W. Basuki, J. Aktaa, Process optimization for diffusion bonding of tungsten with Eurofer97 using a vanadium interlayer, Journal of Nuclear Materials 459 (2015) 217–234.

[10] H. Noto, A. Kimura, H. Kurishita, S. Matsuo, S. Nogami, Evaluation of feasibility of tungsten/oxide dispersion strengthened steel bonding with vanadium insert, Materials Transactions 54 (2013) 451–455.

[11] Z. Zhong, H.-C. Jung, T. Hinoki, A. Kohyama, Effect of joining temperature on the microstructure and strength of tungsten/ferritic steel joints diffusion bonded with a nickel interlayer, Journal of Materials Processing Technology 210 (2010) 1805–1810.

[12] G. Zou, J. Yang, A. Wu, G. Huang, D. Zhang, J. Ren, Q. Wang, Diffusion bonding of tungsten to copper and its alloy with Ti foil and Ti/Ni/Ti multiple interlayers, Journal of Materials Science and Technology 19 (2003) 189–192.

[13] Y.-I. Jung, J.-Y. Park, B.-K. Choi, D.-W. Lee, S. Cho, Interfacial microstructures of HIP joined W and ferritic–martensitic steel with Ti interlayers, Fusion Engineering and Design 88 (2013) 2457–2460.

[14] J.-Y. Park, Y.-I. Jung, B.-K. Choi, D.-W. Lee, S. Cho, Joining of tungsten to ferritic/martensitic steels by hot isostatic pressing, Journal of Nuclear Materials 442 (2013) 541–545.

[15] J.-C. Wang, W. Wang, R. Wei, X. Wang, Z. Sun, C. Xie, Q. Li, G.-N. Luo, Effect of Ti interlayer on the bonding quality of W and steel HIP joint, Journal of Nuclear Materials 485 (2017) 8–14.

[16] W. S. Liu, Q. S. Cai, Y. Z. Ma, Y. Y. Wang, H. Y. Liu, D. X. Li, Microstructure and mechanical properties of diffusion bonded W/steel joint using V/Ni composite interlayer, Materials Characterization 86 (2013) 212–220.

[17] J. Li, X. Fang, J. F. Yang, G.-J. Qiao, Influence of different interlayers metals on properties of diffusion bonding joint of tungsten to copper, Materials Science Forum 620-622 (2009) 65–68.

[18] Q. Cai, W. Liu, Y. Ma, H. Liu, Microstructure, residual stresses and mechanical properties of diffusion bonded tungsten–steel joint using a V/Cu composite barrier interlayer, International Journal of Refractory Metals & Hard Materials 48 (2015) 312–317.

[19] G. Pintsuk, S. E. Brunings, J. E. Doring, J. Linke, I. Smid, L. Xue, Development of W/Cu-functionally graded materials, Fusion Engineering and Design 66-68 (2003) 237–240.

[20] T. Chehtov, J. Aktaa, O. Kraft, Mechanical characterization and modeling of brazed Eurofer-tungsten-joints, Journal of Nuclear Materials 367-370 (2007) 1228–1232.

[21] B. A. Kalin, V. T. Fedotov, O. N. Sevrjukov, A. Moeslang, M. Rohde, Development of rapidly quenched brazing foils to join tungsten alloys with ferritic steel, Journal of Nuclear Materials 329-333 (2004) 1544–1548.

[22] B. A. Kalin, V. T. Fedotov, O. N. Sevrjukov, A. N. Kalashnikov, A. N. Suchkov, A. Moeslang, M. Rohde, Development of brazing foils to join monocrystalline tungsten alloys with ODS-Eurofer steel, Journal of Nuclear Materials 367-370 (2007) 1218–1222.

[23] Y. Ma, Q. Cai, W. Liu, S. Liu, Microstructure and mechanical properties of brazed tungsten/steel joint for divertor applications, Materials Science Forum 789 (2014) 384–390.

[24] P. Gustafson, A thermodynamic evaluation of the C-Fe-W system, Metallurgical Transactions A 18 (1987) 175–188.

[25] Y. Nishi, Y. Mogi, K. Oguri, Preparation of Fe–W amorphous films by an electroplating method, Journal of Materials Science Letters 14 (1995) 1–3.

[26] Y. Itoh, M. Takahashi, H. Takano, Design of tungsten/copper graded composite for high heat flux components, Fusion Engineering and Design 31 (1996) 279–289.

[27] R. Jedamzik, A. Neubrand, J. Rodel, Functionally graded materials by electrochemical processing and infiltration: application to tungsten/copper composites, Journal of Materials Science 35 (2000) 477–486.

[28] Z.-J. Zhou, S.-X. S. J. Du, Z.-H. Zhong, C.-C. Ge, Performance of W/Cu FGM based plasma facing components under high heat load test, Journal of Nuclear Materials 363-365 (2007) 1309–1314.

[29] G. Pintsuk, I. Smid, J. E. Doring, W. Hohenauer, J. Linke, Fabrication and characterization of vacuum plasma sprayed W/Cu-composites for extreme thermal conditions, Journal of Materials Science 42 (2007) 30–39.

[30] N. Tsyntsaru, J. Bobanova, X. Ye, H. Cesiulis, A. Dikusar, I. Prosycevas, J. P. Celis, Iron-tungsten alloys electrodeposited under direct current from citrate-ammonia plating baths, Surface and Coatings Technology 203 (2009) 3136–3141.

[31] Z. Zhou, S. Guo, S. Song, W. Yao, C. Ge, The development and prospect of fabrication of W based plasma facing component by atmospheric plasma spraying, Fusion Engineering and Design 86 (2011) 1625–1629.

[32] T. Weber, Entwicklung und Optimierung von gradierten Wolfram/Eurofer97-Verbindungen für Divertorkomponenten, Ph.D. thesis, Karlsruher Institut für Technologie (2012).

[33] M. M. Gasik, Micromechanical modelling of functionally graded materials, Computation Materials Science 13 (1998) 42–55.

[34] S. Ueda, M. M. Gasik, Thermal-elasto-plastic analysis of W-Cu functionally graded materials subjected to a uniform heat flow by micromechanical model, Journal of Thermal Stresses 24 (2000) 395–409.

[35] T. Weber, J. Aktaa, Numerical assessment of functionally graded tungsten/steel joints for divertor applications, Fusion Engineering and Design 86 (2011) 220–226.

[36] D. Qu, W. W. Basuki, J. Aktaa, Numerical assessment of functionally graded tungsten/Eurofer coating system for first wall applications, Fusion Engineering and Design 98-99 (2015) 1389–1393.

[37] D. Qu, Development of functionally graded tungsten/Eurofer coating systems, Ph.D. thesis, Karlsruher Institut für Technologie (2015).

[38] D. Qu, W. W. Basuki, J. Gibmeier, R. Vaßen, J. Aktaa, Development of functionally graded tungsten/Eurofer coating systems for first wall applications, Fusion Science and Technology 68 (2015) 578–581.

[39] T. Emmerich, D. Qu, R. Vaßen, J. Aktaa, Development of W-coating with functionally graded W/Eurofer-layers for protection of first-wall materials, Fusion Engineering and Design 128 (2018) 58–67.

[40] Y. Igitkhanov, B. Bazylev, R. Fetzer, The quantification of the key physics parameters for the DEMO fusion power reactor and analysis of the reactor relevant physics issues, KIT Scientific Publishing, 2014.

[41] Y. Igitkhanov, R. Fetzer, B. Bazylev, Effect of design geometry of the DEMO first wall on the plasma heat load, Nuclear Materials and Energy 9 (2016) 560–564.

[42] M. Beckers, W. Biel, M. Tokar, U. Samm, Investigations of the first-wall ersosion of DEMO with the CELLSOR code, Nuclear Materials and Engineering 12 (2017) 1163–1170.

[43] M. Beckers, W. Biel, M. Tokar, U. Samm, Investigations of the first-wall erosion of demo with the cellsor code, in: Proceedings of the 22nd International Conference on Plasma Surface Interactions in Controlled Fusion Devices, 2016.

[44] F. Tavassoli, Fusion demo interim design criteria (DISDC)/appendix A: Material design limit data/A3.S18E Eurofer steel, DMN/DIR/NT/2004-000/A, Tech. rep., DMN Technical Report (2004).

[45] ITER Materials Properties Handbook (MPH), ITER Doc. G 74 MA 16 04-05-07 R0.1 (internal project document distributed to the ITER Partic-

ipants), 2017.
[46] P. A. D. Maio, S. Garitta, J. H. You, G. Mazzone, E. Vallone, Analysis of steady state thermal-hydraulic behaviour of the DEMO divertor cassette body cooling circuit, Fusion Engineering and Design 124 (2017) 437–441.
[47] J. H. You, E. D. D. project team, WPDIV: Selected results from recent tasks, in: German DEMO Workshop (Garching), 12.-13. Jan 2017.
[48] M. Merola, G. Vieider, et al, EUPITER: the european thermohydraulic package for plasma facing components, Proceedings of the Specialists' Workshop on High Heat Flux Cooling for ITER PFCs (JET, Culham, UK).
[49] S. Pestchanyi, Simulation of heat flux to the DEMO first wall due to filamentary transport in the far SOL, IEEE Transactions on Plasma Science 46 (2017) 1393–1397.
[50] R. C. Progelhof, J. L. Throne, R. R. Ruetsch, Method for predicting the thermal conductivity of composite systems: A review, Polymer Engineering and Science 16 (1976) 615 – 625.
[51] S. Petit-Grostabussiat, L. Taleb, J.-F. Jullien, Experimental results on classical plasticity of steels subjected to structural transformations, International Journal of Plasticity 20 (2004) 1371–1386.
[52] M. Rieth, M. Schirra, A. Falkenstein, P. Graf, S. Heger, H. Kempe, R. Lindau, H. Zimmermann, Eurofer97 - Tensile, Charpy, Creep and Structural Test, Forschungszentrum Karlsruhe, 2003.